Title

Localization of microbarom sources using the IMS infrasound network

Journal

Journal of Geophysical Research: Atmospheres, 117(D6)

ISSN

01480227

Authors

Landès, Matthieu
Ceranna, Lars
Le Pichon, Alexis
et al.

Publication Date

2012-03-27

DOI

10.1029/2011JD016684

Peer reviewed

Localization of microbarom sources using the IMS infrasound network

Matthieu Landès,[1] Lars Ceranna,[2] Alexis Le Pichon,[1] and Robin S. Matoza[3]

Received 4 August 2011; revised 18 January 2012; accepted 27 January 2012; published 17 March 2012.

[1] Multiyear continuous infrasound monitoring with the global International Monitoring System (IMS) demonstrates that microbaroms, generated by nonlinear interaction of opposing oceanic surface waves, are globally observed at equatorial, middle, and high latitudes. Direction of arrival of microbarom signals are systematically estimated at all IMS infrasound stations. Using a cross-bearing method, we perform a monthly localization of worldwide microbarom sources. At most stations, microbarom detections show clear seasonal trends, driven by stratospheric wind reversals and source effects. Five-year averaging of the detections provides global and statistical observations of seasonal source variations. Our microbarom source locations represent a first attempt to infer ocean swell characteristics from global and long-term measurements. We show that the monthly averaged source locations exhibit clear seasonal switching between the northern and southern hemispheres. Such an approach can help with evaluating the network detection capability, and provides new insights into quantitative relationships between infrasonic observables, atmospheric specifications, and ocean–atmosphere interactions.

Citation: Landès, M., L. Ceranna, A. Le Pichon, and R. S. Matoza (2012), Localization of microbarom sources using the IMS infrasound network, *J. Geophys. Res.*, *117*, D06102, doi:10.1029/2011JD016684.

1. Introduction

[2] The global International Monitoring System (IMS) infrasound network, constructed for compliance with the Comprehensive Nuclear-Test ban Treaty (CTBT), enables continuous monitoring of the atmosphere. In addition to its primary function of detecting nuclear test explosions, the IMS network offers an opportunity to study background noise sources on a global scale [*Hedlin et al.*, 2002]. In turn, such studies permit assessments of the network performance, discrimination of signals of interest, and improvements to atmospheric models [*Le Pichon et al.*, 2010]. Background infrasonic noise is usually characterized by an energy peak between 0.2 and 0.3 Hz associated with so-called microbarom signals. The mechanism of microbarom radiation was first described by *Longuet-Higgins* [1950]. He explained how two waves of the same frequency, with opposite directions of propagation, can generate waves that excite the ocean floor producing microseismic noise [*Hasselmann*, 1963; *Webb and Cox*, 1986; *Webb*, 1992], and radiate acoustic waves in the atmosphere [*Posmentier*, 1967; *Arendt and Fritts*, 2000; *Waxler and Gilbert*, 2006]. In the microbarom frequency band, the waves can propagate thousands of kilometers in atmospheric waveguides with weak attenuation [*Sutherland and Bass*, 2004] and may be a potential heat source in the upper atmosphere [*Rind*, 1977; *Hickey et al.*, 2001].

[3] Detection capability is a key concern with the IMS infrasound network. Microbaroms are known to interfere with the detection of explosive events [e.g., *Evers and Haak*, 2001; *Stevens et al.*, 2002] and to complicate the identification of long-range volcanic eruption signals [e.g., *Matoza et al.*, 2011]. In this context, constraints on microbarom source regions provide useful information for discrimination purposes. Microbarom source region estimates may also be useful for tomography studies. Global and continuous monitoring of microbaroms could allow the vertical structure of high-altitude winds and temperature to be recovered [*Donn and Rind*, 1971]. Previous analyses of observations at individual stations [*Rind and Donn*, 1975; *Garcés et al.*, 2004; *Brachet et al.*, 2010] showed that microbarom detections are essentially driven by the seasonal variations of the stratospheric winds [*Le Pichon et al.*, 2006]. However, estimates of source parameters such as source location and intensity are crucial for using microbarom signals as input in atmospheric remote sensing methods. We note that *Haney* [2009] performed microbarom waveform cross-correlation between infrasound stations separated by 13.5 km to infer local atmospheric structure. The method of *Haney* [2009] does not require the microbarom source location to be known.

[4] Seismological studies also indicate a seasonal variation in the microseism source region using seismic noise recorded by multiple networks [*Gerstoft et al.*, 2008; *Landès et al.*, 2010]. The results of these studies are consistent with numerical simulations from *Kedar et al.* [2008] which

[1]CEA, DAM, DIF, Arpajon, France.
[2]BGR, Hannover, Germany.
[3]Institute of Geophysics and Planetary Physics, Scripps Institution of Oceanography, La Jolla, California, USA.

0148-0227/12/2011JD016684

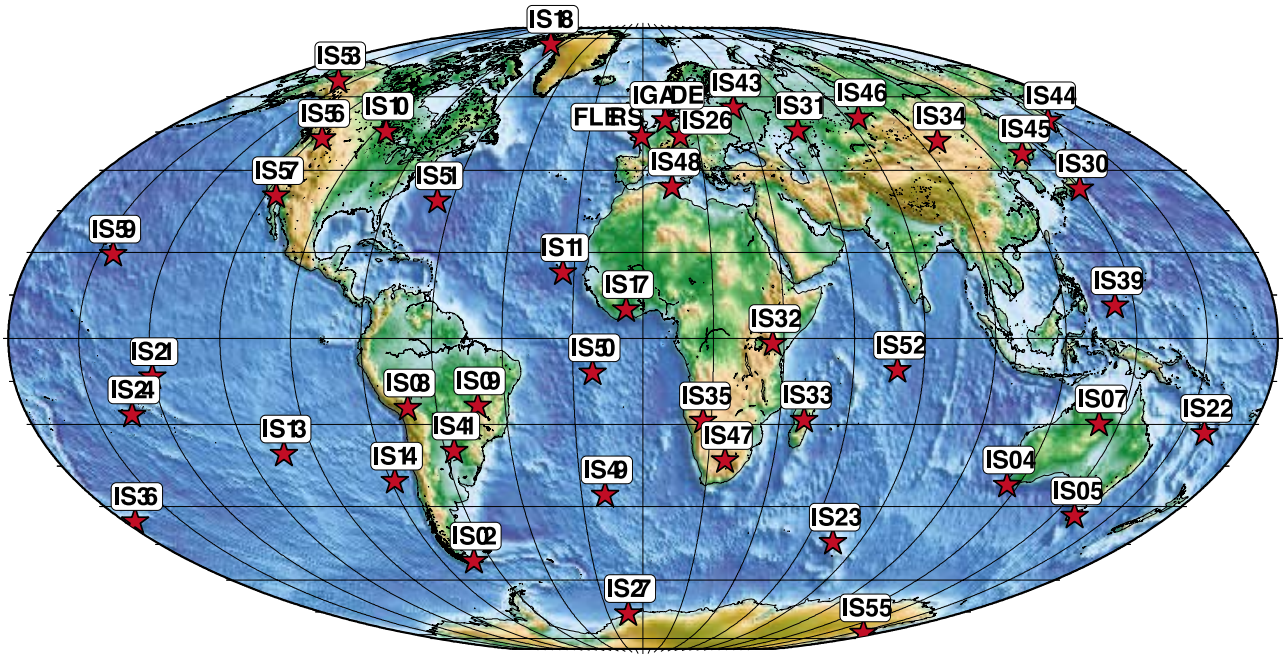

Figure 1. Location map of the 39 IMS stations operational at the time of this study, and additional experimental arrays in France (FLERS) and Germany (IGADE).

combine Longuet-Higgins' theory, wave models and bathymetry to predict the excitation intensity of microseismic surface waves. Following these microseism studies, we present global source locations of microbaroms using a simple cross-bearing approach and five-years of continuous recordings at all IMS stations operating between 2006 and 2010. We then discuss seasonal trends in the reconstructed source regions.

2. Data and Observations

[5] IMS infrasound stations consist of arrays of at least 4 microbarometers with 1 to 3 km aperture. At almost all stations (Figure 1), continuous microbarom signals are detected as quasi-monochromatic signals coherent across the array, with a dominant frequency between 0.2 and 0.3 Hz. The wave parameters (e.g., azimuth, amplitude, apparent velocity and frequency) of these signals are calculated using the Progressive MultiChannel Correlation (PMCC) algorithm [*Cansi*, 1995]. A PMCC "pixel" represents coherent acoustic energy in a single time-frequency bin. Pixels of similar wavefront properties are grouped into "families" [*Cansi*, 1995]. In this paper, a detection is defined as a PMCC family.

[6] The data used in this study include all detections from 39 IMS stations and two additional arrays (FLERS, France; IGADE, Northern Germany) which were also running between 2006 and 2010. In order to clean the detection lists and to discard detections from local sources, a simple categorization procedure is applied [*Brachet et al.*, 2010]. From this data set, we extract long duration detections with frequencies between 0.1 and 0.4 Hz. Furthermore, detections, with a root-mean square (RMS) amplitude that differs by 4 standard deviations or more from the mean amplitude of all detections at each station, are considered as outliers. In addition, detections of poor signal-to-noise-ratio (SNR) are removed (i.e., we keep detections composed of a minimum of 15 pixels [*Cansi and Klinger*, 1997]). Overall, a data set of nearly two million detections is constructed with a median number of 11, 100 detections per station per year.

[7] To estimate the overall quality of microbarom detections for the entire network, we represent in Figure 2 the monthly number of detections at each station between 2006 and 2010. Two stations (IS59 and IS02) have less than one year of continuous recording and 30 stations have more than 3 years. However, the data set used in this study is large enough to perform relevant statistical analyses. The station distribution provides a nearly global coverage and the time period investigated reveals clear seasonal trends. Previous global-scale studies [*Le Pichon et al.*, 2006] have already shown that seasonal variations in observed bearings between northern and southern hemispheres follow to first order the prevailing stratospheric winds. This pattern is confirmed in Figure 3.

3. Methods and Results

[8] Since microbaroms are not impulsive signals but are rather quasi-monochromatic continuous wave trains [*Olson and Szuberla*, 2005], traditional methods for point source location using arrival times cannot be used. We present here a simple cross-bearing approach aiming to statistically reconstruct the main source regions. Monthly global location maps are computed following a three-step procedure:

[9] 1. At a given station S, the weighting function P_S^d determines the confidence for a point M to be the source of the detection d. At station M, this function is written as:

$$P_S^d(M) = \begin{cases} 1 & \text{if } |\theta^d - \theta_{SM}| < 5^\circ \text{ and } \Delta(S,M) < 10,000\,\text{km} \\ 0 & \text{otherwise} \end{cases} \quad (1)$$

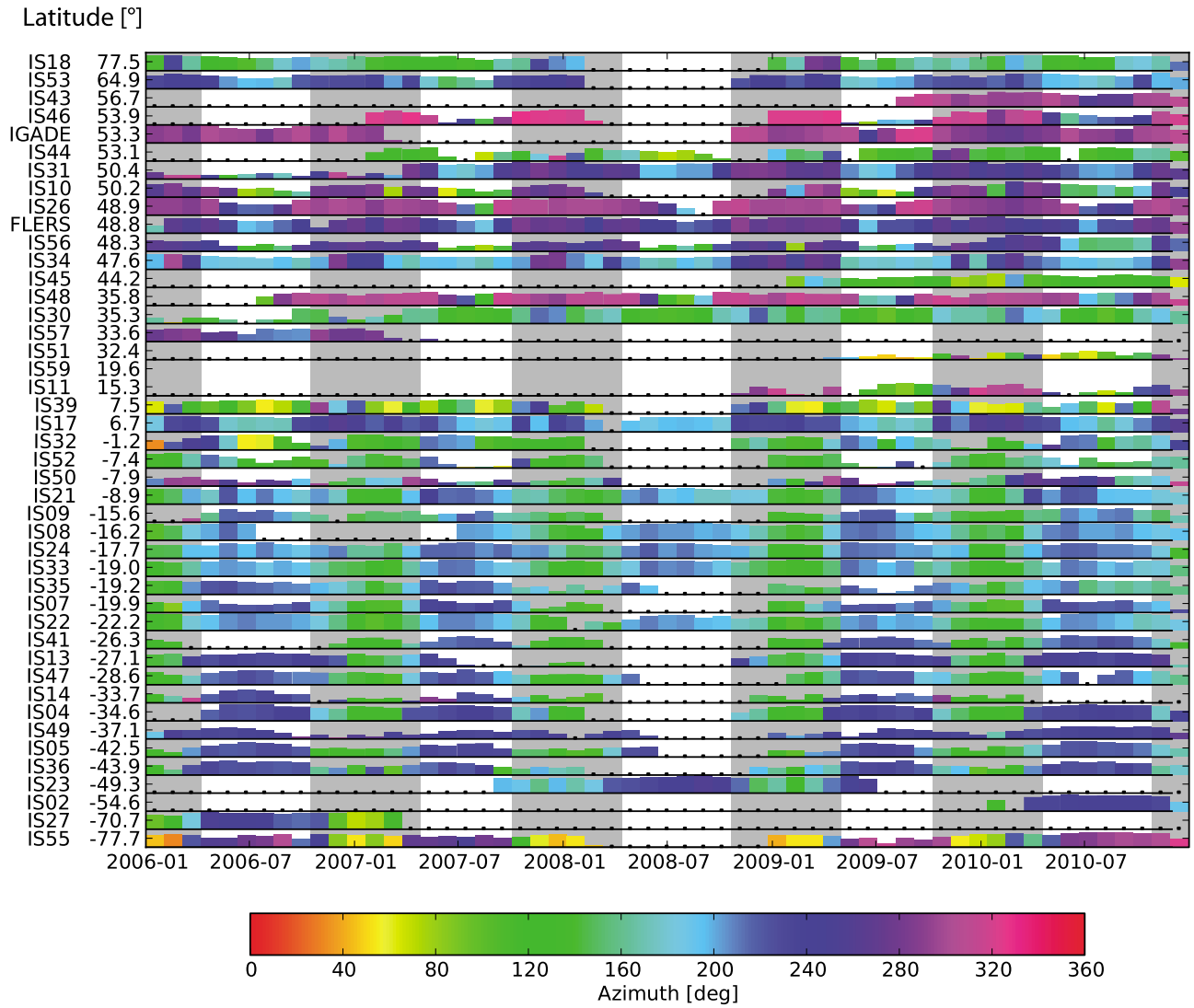

Figure 2. Monthly distribution of number of detections for all stations. Stations are sorted by latitude. Detections are counted in log scale. For each station, the upper limit of the y axis corresponds to 15,000 detections. The color codes the average azimuth of detections. The vertical gray bars correspond to northern hemisphere winter (October to March). Small black dots indicate lack of data.

where θ^d is the back-azimuth of the detection d as seen from station S, $\Delta(S, M)$ and θ_{SM} are the distance and the azimuth of the great circle path between S and M respectively. This function defines a sector on the Earth centered on the detected back-azimuth with a width of 10° and a radial distance of 10,000 km. The angle of 10° accounts for uncertainties resulting from the combined effects of both the array response at a typical IMS station of 1–3 km aperture [*Szuberla and Olson*, 2004] and propagation effects [e.g., *Le Pichon et al.*, 2005; *Antier et al.*, 2007].

[10] 2. Then, we define the function P_S proportional to the probability of a source location at a point M generating signals that are detected at station S:

$$P_S(M) = k \sum_{d \in E_S} P_S^d(M) \tag{2}$$

where E_S is the set of all detections recorded at station S, and k is a normalization factor such that

$$\max_{M \in \text{Earth}} \{P_S(M)\} = 1 \tag{3}$$

[11] 3. Finally, the distribution P of the microbarom source is the summation of P_S functions weighted by a factor f_S over all stations. For a point M on the Earth, we have:

$$P(M) = q \sum_S f_S P_S(M) \tag{4}$$

where q is such that $\max\{P\} = 1$.

[12] To evaluate f_S, we use the number of pixels, which provides indications of the area of the detection in the time-frequency domain [*Cansi*, 1995]. f_S is defined by the average of the number of pixels for all detections in E_S.

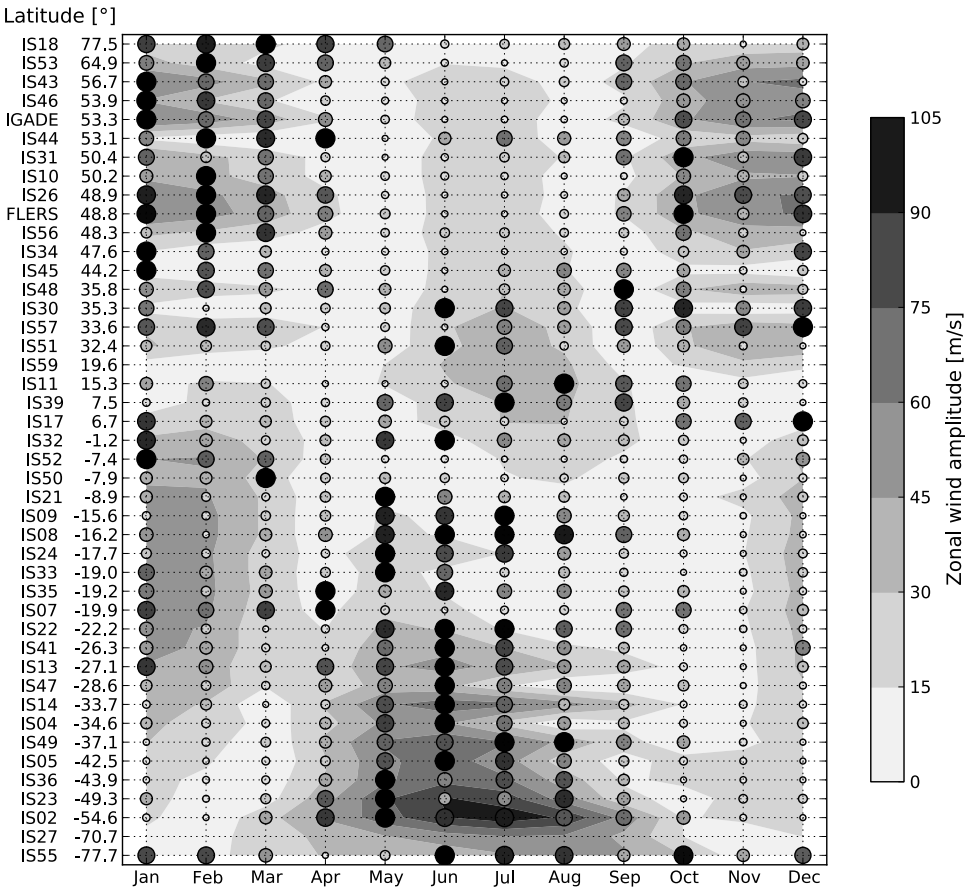

Figure 3. Monthly distribution of number of detections for all stations. The size and the color of the circles are related to the logarithm of the number of detections (normalized for each station). The color of the shaded areas codes zonal stratospheric wind strength predicted by the HWM07 [*Drob et al.*, 2008] wind model (computed on the 15th of each month at 40 km altitude).

[13] The resulting location maps correspond to the function P evaluated on a $1^\circ \times 1^\circ$ global grid in latitude and longitude.

[14] The monthly averaged spatial distributions of microbarom sources are shown in Figure 4. Artifacts in the locations, induced by the effects of poor azimuthal coverage and the 10° uncertainties, are visible in Antarctica (especially in March, October and November) and in North America (in August and September), where the method shows sources over land. These maps clearly show large seasonal trends, with dominating microbarom sources in the northern hemisphere during the boreal winter, and dominating sources in the southern hemisphere during the austral winter. The location maps exhibit different structures between the two hemispheres. In the northern hemisphere, sources are mainly concentrated in the Atlantic Ocean, south of Greenland, and in the northern Pacific Ocean. In the southern hemisphere, sources are distributed fairly uniformly along the peri-Antarctic belt, between 45°S and 60°S. The variability in intensity of these source regions may correspond to real variability in the rate of microbarom generation, but may also be partially explained by the non-homogeneous network coverage. Furthermore, during the equinox periods, locations are poorly constrained. The lack of precision is likely due to unstable stratospheric waveguides, which inhibit long-range propagation, resulting in fewer detections and weaker SNR (Figure 2). This observation is consistent with previous detection capability studies of the IMS network [*Le Pichon et al.*, 2009; *Green and Bowers*, 2010], which predict an increase of the detection thresholds during the equinox periods when stratospheric winds reduce and reverse.

[15] Several factors introduce uncertainties in the location maps. In particular, the local environment and array configuration may explain large differences in the number of detections. In order to avoid these effects, equation (4) defines a normalization factor for each station. Therefore, our location maps depend on the number of intersected beams, rather than the number of detections. The resulting maps do not track ocean swells but reflect the global distribution of microbaroms sources radiating acoustic energy. To compensate bias introduced by the less detections at some stations, the location results are monthly averaged, enhancing seasonal trends and smoothing the source regions.

[16] Since back azimuths are not wind-corrected, errors are introduced in the location procedure. However, the use of a 10° range of uncertainty (equation (1)) is intended to account for these errors. Despite the relatively simplistic approach proposed, the located source regions are fairly well constrained and are generally not above the continents. Moreover, location results are even more realistic and

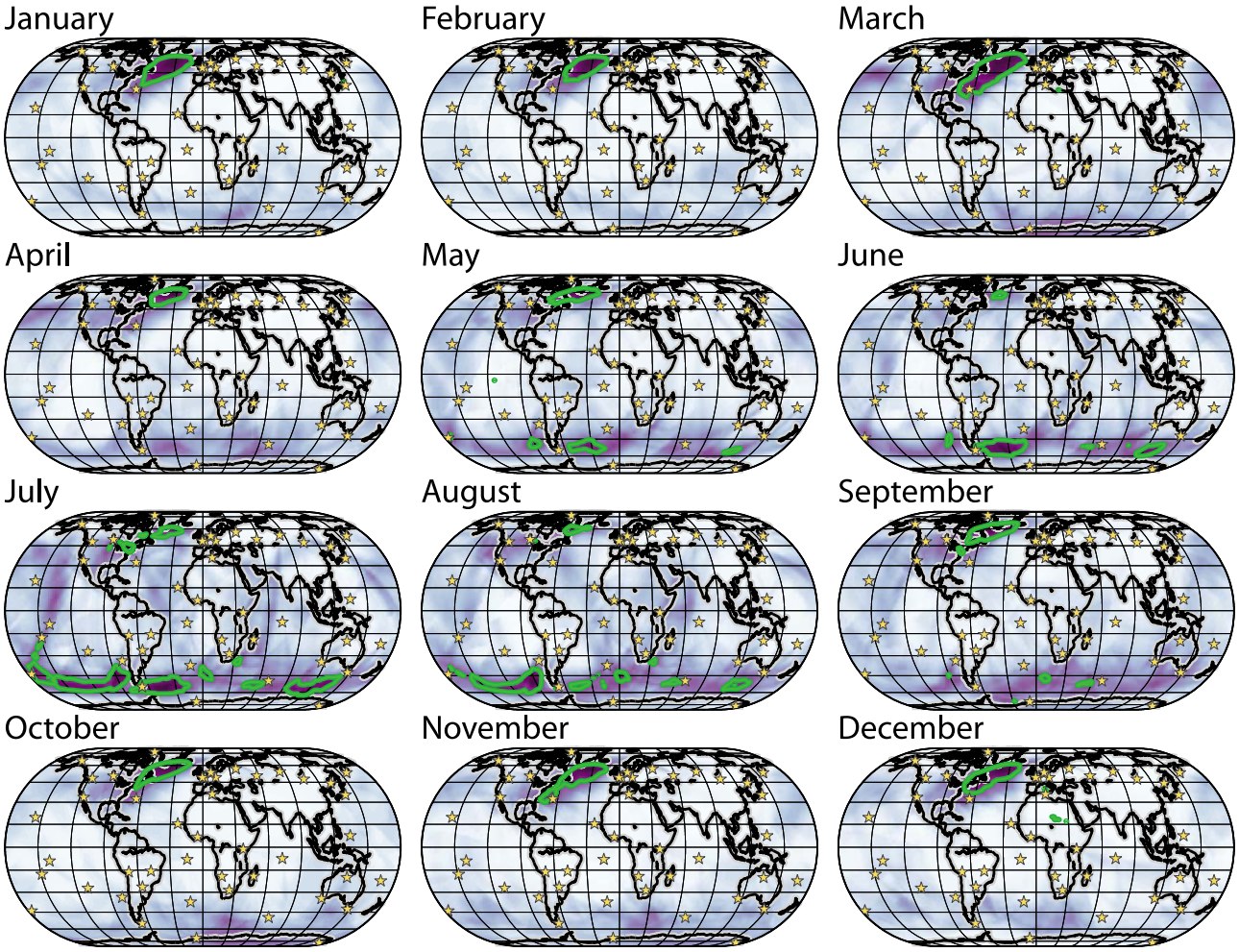

Figure 4. Monthly location of microbarom sources. The green contour level delimits regions where the function P is higher than 0.7. Dark purple color corresponds to a high probability while white is associated to null probability.

consistent when limited to areas defined by $P = 0.7$ (green contour levels on Figure 4). This threshold is arbitrarily chosen and does not have any physical interpretation. However, the global coverage of the network and the large time period covered give confidence to our location maps with clear seasonal trends consistent over the five years. This monthly averaging approach reduces the influence of episodic storms and therefore provides reliable location estimates of the dominating microbarom source regions.

4. Concluding Remarks

[17] Our maps are qualitatively consistent with seasonal climatic trends. The dominant sources follow the north-south variations in ocean storm activity in both hemispheres, which can be observed in models of oceanic wave height (e.g., NOAA Wavewatch III, http://polar.ncep.noaa.gov/waves). Since larger waves means larger microbarom signals, there is some correlation between wave activity and regions of significant microbarom generation. However, large waves are not enough. The commonly accepted source mechanism for microbarom signals described by *Waxler and Gilbert* [2006] is based on nonlinear interactions of counter propagating waves [*Longuet-Higgins*, 1950].

[18] Following single station studies [e.g., *Willis et al.*, 2004; *Le Pichon et al.*, 2006], our network processing results permit global connection of microbarom observations to infer ocean-atmosphere interaction processes. Future work should compare our locations with numerical estimates of microbarom source amplitudes using Longuet-Higgins' theory. Estimates of the wave interaction term have already been evaluated numerically to estimate microseism excitation in the northern hemisphere [*Kedar et al.*, 2008] and study infrasound signals generated by cyclones [*Stopa et al.*, 2011].

[19] As already shown by *Donn and Naini* [1973] and *Rind* [1980] our results provide additional evidence that both microseismic noise and microbaroms originate from the same nonlinear source mechanism. Due to uncertainties in our location process regarding both propagation and multi-year averaging effects, and considering that a convincing model for the influence of bathymetry on the microbarom source mechanism has not yet appeared in the literature [*Waxler and Gilbert*, 2006], only qualitative comparisons with seismic results can be made. However, we note that

microbarom and microseism sources are always in the open ocean and follow the same seasonal trends between the northern and southern hemispheres. In addition, location patterns are comparable in the northern hemisphere winter when the area south of Greenland is the dominant source region of both microseisms and microbaroms [*Landès et al.*, 2010].

[20] In conclusion, a multiyear analysis of low-frequency detections on the IMS network allows the investigation of seasonal trends in the global distribution of microbarom source regions. Clear seasonal variations in the source locations are observed. They highlight the potential of combined microseismic and microbarom studies to improve the knowledge of the same source mechanism over the deep ocean. In order to improve our location maps, further work would account for the effect of high altitude winds on the detected azimuths. Comparisons with numerical models combining intensity of wave interactions and atmospheric propagation models should also be performed.

References

Antier, K., A. Le Pichon, S. Vergniolle, C. Zielinski, and M. Lardy (2007), Multiyear validation of the NRL-G2S wind fields using infrasound from Yasur, *J. Geophys. Res.*, *112*, D23110, doi:10.1029/2007JD008462.

Arendt, S., and D. C. Fritts (2000), Acoustic radiation by ocean surface waves, *J. Fluid Mech.*, *415*, 1–21.

Brachet, N., D. Brown, R. Le Bras, Y. Cansi, P. Mialle, and J. Coyne (2010), Monitoring the Earth's atmosphere with the Global IMS Infrasound Network, in *Infrasound Monitoring for Atmospheric Studies*, edited by A. Le Pichon, E. Blanc, and A. Hauchecorne, pp. 77–118, Springer, New York.

Cansi, Y. (1995), An automatic seismic event processing for detection and location: The P.M.C.C. method, *Geophys. Res. Lett.*, *22*, 1021–1024, doi:10.1029/95GL00468.

Cansi, Y., and Y. Klinger (1997), An automated data processing method for mini-arrays, *CSEM/EMSC Newsl.*, *11*, 2–4.

Donn, W. L., and B. Naini (1973), Sea wave origin of microbaroms and microseisms, *J. Geophys. Res.*, *78*, 4482–4488, doi:10.1029/JC078i021p04482.

Donn, W. L., and D. Rind (1971), Natural infrasound as an atmospheric probe, *Geophys. J. Int.*, *26*, 111–133, doi:10.1111/j.1365-246X.1971.tb03386.x.

Drob, D. P., et al. (2008), An empirical model of the Earth's horizontal wind fields: HWM07, *J. Geophys. Res.*, *113*, A12304, doi:10.1029/2008JA013668.

Evers, L. G., and H. W. Haak (2001), Listening to sounds from an exploding meteor and oceanic waves, *Geophys. Res. Lett.*, *28*, 41–44, doi:10.1029/2000GL011859.

Garcés, M., M. Willis, C. Hetzer, A. Le Pichon, and D. Drob (2004), On using ocean swells for continuous infrasonic measurements of winds and temperature in the lower, middle, and upper atmosphere, *Geophys. Res. Lett.*, *31*, L19304, doi:10.1029/2004GL020696.

Gerstoft, P., P. M. Shearer, N. Harmon, and J. Zhang (2008), Global P, PP, and PKP wave microseisms observed from distant storms, *Geophys. Res. Lett.*, *35*, L23306, doi:10.1029/2008GL036111.

Green, D. N., and D. Bowers (2010), Estimating the detection capability of the International Monitoring System infrasound network, *J. Geophys. Res.*, *115*, D18116, doi:10.1029/2010JD014017.

Haney, M. M. (2009), Infrasonic ambient noise interferometry from correlations of microbaroms, *Geophys. Res. Lett.*, *36*, L19808, doi:10.1029/2009GL040179.

Hasselmann, K. (1963), A statistical analysis of the generation of microseisms, *Rev. Geophys.*, *1*, 177–210, doi:10.1029/RG001i002p00177.

Hedlin, M. A. H., M. Garces, H. Bass, C. Hayward, G. Herrin, J. Olson, and C. Wilson (2002), Listening to the secret sounds of Earth's atmosphere, *Eos Trans. AGU*, *83*, 564–565, doi:10.1029/2002EO000383.

Hickey, M. P., G. Schubert, and R. L. Walterscheid (2001), Acoustic wave heating of the thermosphere, *J. Geophys. Res.*, *106*, 21,543–21,548, doi:10.1029/2001JA000036.

Kedar, S., M. Longuet-Higgins, F. Webb, N. Graham, R. Clayton, and C. Jones (2008), The origin of deep ocean microseisms in the North Atlantic Ocean, *Proc. R. Soc., Ser. A*, *464*, 777–793, doi:10.1098/rspa.2007.0277.

Landès, M., F. Hubans, N. M. Shapiro, A. Paul, and M. Campillo (2010), Origin of deep ocean microseisms by using teleseismic body waves, *J. Geophys. Res.*, *115*, B05302, doi:10.1029/2009JB006918.

Le Pichon, A., E. Blanc, D. Drob, S. Lambotte, J. X. Dessa, M. Lardy, P. Bani, and S. Vergniolle (2005), Infrasound monitoring of volcanoes to probe high-altitude winds, *J. Geophys. Res.*, *110*, D13106, doi:10.1029/2004JD005587.

Le Pichon, A., L. Ceranna, M. Garcés, D. Drob, and C. Millet (2006), On using infrasound from interacting ocean swells for global continuous measurements of winds and temperature in the stratosphere, *J. Geophys. Res.*, *111*, D11106, doi:10.1029/2005JD006690.

Le Pichon, A., J. Vergoz, E. Blanc, J. Guilbert, L. Ceranna, L. Evers, and N. Brachet (2009), Assessing the performance of the International Monitoring System's infrasound network: Geographical coverage and temporal variabilities, *J. Geophys. Res.*, *114*, D08112, doi:10.1029/2008JD010907.

Le Pichon, A., E. Blanc, and A. Hauchecorne (Eds.) (2010), *Infrasound Monitoring for Atmospheric Studies*, Springer, New York.

Longuet-Higgins, M. S. (1950), A theory of the origin of microseisms, *Philos. Trans. R. Soc.*, *Ser. A*, *243*, 1–35, doi:10.1098/rsta.1950.0012.

Matoza, R. S., et al. (2011), Long-range acoustic observations of the Eyjafjallajökull eruption, Iceland, April–May 2010, *Geophys. Res. Lett.*, *38*, L06308, doi:10.1029/2011GL047019.

Olson, J. V., and C. A. L. Szuberla (2005), Distribution of wave packet sizes in microbarom wave trains observed in Alaska, *J. Acoust. Soc. Am.*, *117*, 1032–1037, doi:10.1121/1.1854651.

Posmentier, E. S. (1967), A theory of microbaroms, *Geophys. J. Int.*, *13*, 487–501, doi:10.1111/j.1365-246X.1967.tb02301.x.

Rind, D. (1977), Heating of the lower thermosphere by the dissipation of acoustic waves, *J. Atmos. Terr. Phys.*, *39*, 445–456.

Rind, D. (1980), Microseisms at Palisades: 3. Microseisms and microbaroms, *J. Geophys. Res.*, *85*, 4854–4862, doi:10.1029/JB085iB09p04854.

Rind, D., and W. L. Donn (1975), Further use of natural infrasound as a continuous monitor of the upper atmosphere, *J. Atmos. Sci.*, *32*, 1694–1704, doi:10.1175/1520-0469(1975)032<1694:FUONIA>2.0.CO;2.

Stevens, J. L., I. I. Divnov, D. A. Adams, J. R. Murphy, and V. N. Bourchik (2002), Constraints on infrasound scaling and attenuation relations from Soviet explosion data, *Pure Appl. Geophys.*, *159*, 1045–1062, doi:10.1007/s00024-002-8672-4.

Stopa, J. E., K. F. Cheung, M. A. Garcés, and D. Fee (2011), Source of microbaroms from tropical cyclone waves, *Geophys. Res. Lett.*, *38*, L05602, doi:10.1029/2010GL046390.

Sutherland, L. C., and H. E. Bass (2004), Atmospheric absorption in the atmosphere up to 160 km, *J Acoust. Soc. Am.*, *115*, 1012–1032, doi:10.1121/1.1631937.

Szuberla, C. A. L., and J. V. Olson (2004), Uncertainties associated with parameter estimation in atmospheric infrasound arrays, *J Acoust. Soc. Am.*, *115*, 253–258, doi:10.1121/1.1635407.

Waxler, R., and E. K. Gilbert (2006), The radiation of atmospheric microbaroms by ocean waves, *J Acoust. Soc. Am.*, *119*, 2651–2664, doi:10.1121/1.2191607.

Webb, S. C. (1992), The equilibrium oceanic microseism spectrum, *J Acoust. Soc. Am.*, *92*, 2141–2158, doi:10.1121/1.405226.

Webb, S. C., and C. S. Cox (1986), Observations and modeling of seafloor microseisms, *J. Geophys. Res.*, *91*, 7343–7358, doi:10.1029/JB091iB07p07343.

Willis, M., M. Garcés, C. Hetzer, and S. Businger (2004), Infrasonic observations of open ocean swells in the Pacific: Deciphering the song of the sea, *Geophys. Res. Lett.*, *31*, L19303, doi:10.1029/2004GL020684.

L. Ceranna, BGR, Stilleweg 2, D-30655 Hannover, Germany. (lars.ceranna@bgr.de)

M. Landès and A. Le Pichon, CEA, DAM, DIF, F-91297 Arpajon, France. (matthieu.landes@cea.fr; alexis.le-pichon@cea.fr)

R. S. Matoza, Institute of Geophysics and Planetary Physics, Scripps Institution of Oceanography, University of California, San Diego, IGPP 0225, La Jolla, CA 92093-0225, USA. (rmatoza@ucsd.edu)